Metrologia

PAPER • OPEN ACCESS

Development and implementation of an automated four-terminal-pair Josephson impedance bridge

To cite this article: Yaowaret Pimsut *et al* 2024 *Metrologia* **61** 025007

OPEN ACCESS
IOP Publishing | Bureau International des Poids et Mesures Metrologia
Metrologia **61** (2024) 025007 (11pp) https://doi.org/10.1088/1681-7575/ad2539

Development and implementation of an automated four-terminal-pair Josephson impedance bridge

Yaowaret Pimsut[1,2,*], **Stephan Bauer**[1], **Marco Kraus**[1], **Ralf Behr**[1], **Mattias Kruskopf**[1], **Oliver Kieler**[1] and **Luis Palafox**[1]

[1] Physikalisch-Technische Bundesanstalt (PTB), Bundesallee 100, 38116 Braunschweig, Germany
[2] National Institute of Metrology Thailand (NIMT), 3/4-5 Moo 3, Klong 5, Klong Luang, 12120 Pathumthani, Thailand

E-mail: yaowaret.pimsut.ext@ptb.de

Received 30 November 2023, revised 30 January 2024
Accepted for publication 2 February 2024
Published 19 February 2024

CrossMark

Abstract

The four-terminal-pair impedance bridge using pulse-driven Josephson voltage standards at PTB has been fully automated. The same bridge configuration was employed to determine R:R and C:C ratios over the frequency range between 53 Hz to 50 kHz. Only minor changes are needed to cover this large frequency range: amplifiers to increase the sensitivity of the current detections for low frequencies and signal generators with higher resolution at high frequencies to reach 50 kHz. Furthermore, the bridge can be operated for quadrature R:$(1/\omega C)$ measurements. The combined standard uncertainties ($k = 1$) for the new bridge were evaluated for all operating frequencies. They reach $2\,\mathrm{nF\,F^{-1}}$ and $4\,\mathrm{n\Omega\,\Omega^{-1}}$ at 1233.15 Hz. At this frequency, the 10 nF:10 nF ratio matched the ratio of PTB's bridge employing inductive voltage dividers within $1\,\mathrm{nF\,F^{-1}} \pm 3\,\mathrm{nF\,F^{-1}}$ ($k = 1$). Over 45 days, the 10 nF:10 nF ratio deviated less than $-2\,\mathrm{nF\,F^{-1}} \pm 3\,\mathrm{nF\,F^{-1}}$ ($k = 1$). The 12.9 kΩ:10 kΩ ratio at 53 Hz differed $-2\,\mathrm{n\Omega\,\Omega^{-1}} \pm 5\,\mathrm{n\Omega\,\Omega^{-1}}$ ($k = 1$) from the DC ratio measured by the PTB's cryogenic current comparator bridge. Using a 12.9 kΩ resistance standard and a graphene AC quantum Hall resistance, the 10 nF:10 nF ratios derived from quadrature measurements agreed with the PTB's inductive voltage divider bridge better than $9\,\mathrm{nF\,F^{-1}} \pm 13\,\mathrm{nF\,F^{-1}}$ ($k = 1$).

Keywords: impedance measurement, quantized Hall resistor, coaxial impedance bridge, graphene, Josephson arbitrary waveform synthesizer, pulse-driven Josephson voltage standard

1. Introduction

Accurate impedance measurements play a crucial role in various scientific and industrial applications. Impedance bridges are essential tools widely used to determine all kinds of impedance ratios [1]. To ensure the reliability of impedance bridges, standards, and measuring devices, a series of calibrations are performed to establish their traceability to the Système International d'Unités (SI) for impedance units, such as ohm (Ω), farad (F), and henry (H). At the top of these calibration chains, primary standards like a DC quantized Hall resistance (QHR) standard, AC QHR, or a Thompson-Lampard calculable capacitor are employed.

Various national metrology institutes apply similar measurement chains, although there may be slight variations in their approaches. Most of these institutes predominantly

* Author to whom any correspondence should be addressed.

utilize bridges based on transformers and inductive voltage dividers (IVDs). Although the IVD-based bridge provides highly accurate results [2–4], it requires a skilled operator due to the complex measurement networks and long measurement chains. Additionally, these bridges are limited by fixed voltage ratios, phase angles, and signal frequencies for their measurement capabilities.

In 2010, Physikalisch-Technische Bundesanstalt (PTB) introduced an impedance bridge employing programmable Josephson voltage standards (PJVS) [5]. The two-terminal-pair bridge was implemented to measure resistance and capacitance ratios up to 10 kHz frequency. The evaluation of these bridges shows uncertainties of a few parts in 10^8 [5, 6]. Additionally, Palafox *et al* conducted quadrature measurements of a resistor to a capacitor. Since the PJVS bridge uses square waves, it is only balanced at the fundamental tone. The unbalanced higher harmonics limit the sensitivity setting of the lock-in-amplifier and result in lower uncertainties at the order of 10^{-6} [7].

This limitation can be avoided by using Josephson arbitrary waveform synthesizers (JAWS) or pulse-driven Josephson voltage standards, which are an advancement in the voltage metrology field, as documented in [8–12]. It produces highly accurate quantum-based voltage waveforms with excellent amplitude stability over time. It generates pure sine waves without transients, outperforming PJVS regarding spectral purity. Integrating either PJVS or JAWS into impedance bridges has showcased their adaptability and effectiveness in impedance metrology applications.

PTB's four-terminal-pair (4TP) Josephson impedance bridge based on JAWS was introduced by Bauer *et al* [13]. A prominent advantage of using 4TP connections is its substantial enhancement of measurement accuracy, as errors from circuit cables and connectors are significantly reduced by defining current and voltage arms separately. This advantage is particularly significant when measuring the low impedance range, typically in the kOhm range or below.

The 4TP Josephson impedance bridge can be operated for various measurements. These include:

1. ratio measurement such as capacitor-to-capacitor (C:C) and resistor-to-resistor (R:R),
2. quadrature measurement of resistor-to-capacitor (R:$(1/\omega C)$),
3. direct comparison of an impedance standard to a graphene AC QHR.

The preliminary results of the 4TP Josephson impedance bridge from the latter configuration were presented in the work of Bauer *et al* [13].

Additional research involved a collaboration with the Istituto Nazionale di Ricerca Metrologica (INRIM) and the Politecnico di Torino (POLITO), Italy, resulting in an extensive assessment of the 4TP Josephson impedance bridge, as reported in Marzano *et al* [14]. We performed on-site comparisons between PTB's Josephson impedance bridge and INRIM-POLITO's digital impedance bridge. The work focused on ratio measurements at 1233.15 Hz and 2466.3 Hz. Moreover, quadrature and R:R measurements were performed at 1233.15 Hz relative to a graphene AC QHR system. The comparison results and the associated uncertainties demonstrated the best agreement between the two bridges within a few parts in 10^8.

This paper presents the results of capacitance ratio and resistance ratio measurements conducted across a wide frequency range from 53 Hz to 50 kHz. Additionally, it explores the outcomes derived from the quadrature measurements and the direct comparison of impedances to the graphene AC QHR. Furthermore, the uncertainties of the measurements were fully investigated.

2. Measurement setup

Figure 1 provides a schematic representation of the basic setup of the 4TP Josephson impedance bridge. The bridge employs the JAWS system as its voltage sources, current sources, Kelvin network, output detectors, and components such as transformers and equalizers. For low-frequency measurements, additional pre-amplifiers are used in front of D_{HP1} and D_{HP2} to increase the sensitivity of the current detection for the balancing procedure. The bridge was configured for full automation during the ratio and quadrature measurements.

2.1. Josephson impedance bridge

The bridge setup utilizes two independent but synchronized Josephson junction arrays to provide U_1 and U_2 for the impedance standards Z_1 and Z_2, respectively. The operation involves interchanging JAWS voltage to each impedance. To facilitate automated source switching, we employed a universal coaxial multiplexer [15]. This multiplexer consists of four independent coaxial switches that connect the JAWS system to the bridge at the high-potential (HP) arms and can be controlled remotely via optical fibers.

To satisfy the current equalization of the bridge, two active equalizers are incorporated in the bridge, indicated as black circles [2, 16]. The first equalizer is between JAWS1's output and the coaxial switches. The second equalizer is placed between the low-potential (LP) arm, LP2, and the ultra-low noise AC-preamplifier before D_2.

Transformers are essential for the balancing procedures, functioning as detection and injection devices. Two different types are used for the following purposes:

1. Two 100:1 detection transformers, each paired with a lock-in amplifier (LIA) denoted as D_{HP1} and D_{HP2}. These setups are utilized for current detection in the HP arms.
2. Two 1:1 transformers are used with the sources S_1 and S_2. Each of these is coupled with a 10 kΩ resistor. These configurations produce currents into the high-current (HC) arms.
3. A 100:1 injection transformer integrated with a LIA as the Kelvin source S_{K} and a resistive divider. This combination generates current at the low-current (LC) arms.

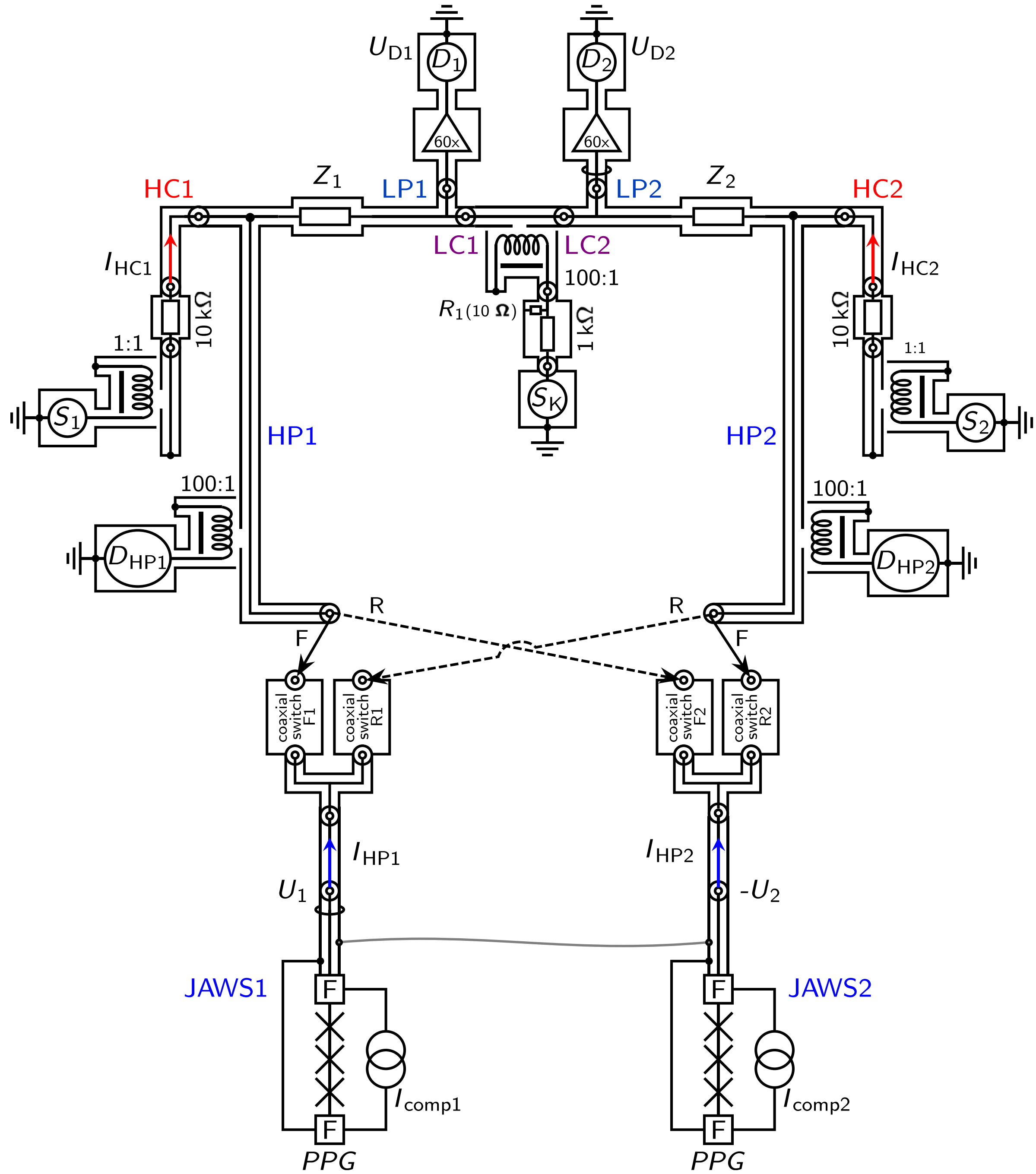

Figure 1. Schematic diagram of the 4TP Josephson impedance bridge setup for ratio measurements of two impedance standards Z_1 and Z_2. JAWS1 and JAWS2 as the voltage sources are connected via coaxial switches at the high-potential terminals, HP1 and HP2. The adjustable currents, I_{HC1} and I_{HC2}, are provided by sources S_1 and S_2, at the high-current terminals, HC1 and HC2. Adjustments to these currents are made until null readings are received by detectors D_{HP1} and D_{HP2}. The Kelvin source S_{K} injects a current to the low-current terminals, LC1 and LC2. The Kelvin current is fine-tuned to null the net currents at the low-potential terminals, LP1 and LP2. As a result, the outputs become equal. These outputs are then amplified by a factor of 60 and simultaneously detected by D_1 and D_2.

In the upper section of the figure 1, the LP arms, LP1 and LP2, the outputs from the Z_1 and Z_2 are amplified by ultra-low noise amplifiers. These 60-fold amplified signals are then detected by two LIAs, D_1 and D_2, yielding U_{D1} and U_{D2} as their outputs. Before reading the output values, each LIA is individually adjusted to an appropriate phase. This process involves applying two different voltages, one at the nominal value and the other set at the nominal voltage plus an additional $100\,\mu\mathrm{V\,V}^{-1}$. By switching between these applied voltages, we can precisely adjust the phase of the LIA until there is no change in the imaginary component of the reading. This step ensures the accuracy of the real part of the output. Furthermore, we can calculate sensitivity coefficients for each detector arm with this well-defined voltage jump of $100\,\mu\mathrm{V\,V^{-1}}$. These coefficients indicate how the bridge responds to the changes in impedance or voltage ratios. The real part and the sensitivity coefficients are essential in the subsequent ratio calculations.

The voltage for each JAWS can be individually set to match specific impedance ratios, offering measurements ranging from 1:1 to 1:10. Additionally, it is flexible to configure the phase angle between the two voltages, facilitating quadrature measurements using the same setup without additional components. In contrast, a conventional quadrature bridge involves more complex networks than the Josephson impedance bridge.

The bridge is fully automated, including the control of the JAWS, execution of balancing processes, frequency sweeping, and calculation of measured ratios. However, it is essential to configure and input the required parameters, such as JAWS bias parameters at each frequency, into the software. The duration for a ratio measurement varies from 5 min to 25 min, depending on the frequency, measured impedance, and ratio.

It is essential to state that, in this work, only C:C and R:R measurements were carried out with the automated bridge. Measurements with the graphene AC QHR and R:$(1/\omega C)$ were performed utilizing a previous bridge configuration. This configuration differs slightly from the one illustrated in figure 1 in that detectors D_{HP1} and D_{HP2} are positioned before the switches and incorporated semi-automated processes. Manual procedures were employed for the balancing steps, and the cable corrections were not included in the reported results since the quadrature and QHR-related measurements are a work in progress with the automated bridge. More details of this alternative bridge configuration can be found in [13].

2.2. Pulse-driven Josephson voltage system

Two JAWS arrays, each comprising 12 000 Josephson junctions (depicted as X in figure 1), were employed. A detailed discussion on the design of PTB's Josephson junction arrays by Kieler *et al* can be found in [17].

We implement the AC coupling technique described by Benz *et al* to generate high-purity sinusoidal waveforms from the JAWS system [18]. High-frequency current pulses are delivered to each array by a pulse pattern generator (PPG), operating at a clock rate of approximately 13 GHz. To achieve the desired output amplitudes, additional compensation currents (I_{comp1} and I_{comp2}) are applied to the arrays. These currents are generated using two waveform generators, each isolated by a transformer at the output.

All bias parameters are optimized to enhance signal accuracy until the quantum-locking range is measured to be 1 mA at an RMS voltage of 100 mV. For a comprehensive understanding of the JAWS system utilized in the impedance bridge, refer to the work by Bauer *et al* [10, 13].

2.3. Balancing procedure

The balancing processes entail a series of iterative adjustments until the bridge satisfies all required conditions. This task, conducted after applying nominal U_1 and U_2 to the impedances, involves the following steps:

1. Injecting currents I_{HC1} and I_{HC2} from sources S_1 and S_2 into the HC terminals. Adjust the amplitudes and phases of the injected currents until the detected currents at D_{HP1} and D_{HP2} are zero (within the resolution of the detectors). This process fulfills the criterion of maintaining zero net current between the inner and outer conductors in the HP arms.
2. Performing the Kelvin balance to bring the net current at LP terminals to zero and to minimize the difference between the LP1 and LP2 output readings. These conditions can be achieved by adjusting the amplitude and phase of the source S_{K}.
3. Proceeding to the main balance by adjusting the amplitude and phase of U_2 until the detected outputs U_{D1} and U_{D2} are close to zero.

The impedance ratio is calculated using the following formula:

$$\frac{Z_2}{Z_1} = \frac{U_2}{U_1}\left[1 + \frac{1}{2}\left(\frac{U_{\mathrm{D1}}}{S_{\mathrm{N1}}} + \frac{U_{\mathrm{D2}}}{S_{\mathrm{N2}}}\right) + \frac{1}{2}\left(\frac{U_{\mathrm{D1}}}{S_{\mathrm{K1}}} - \frac{U_{\mathrm{D2}}}{S_{\mathrm{K2}}}\right)\right]. \tag{1}$$

Where S_{N1} and S_{N2} are the sensitivity coefficients of the bridge networks for Z_1 and Z_2, and S_{K1} and S_{K2} are the coefficients for the Kelvin injection network.

When the bridge is perfectly balanced, with U_{D1} and U_{D2} being zero, equation (1) is simplified to:

$$\frac{Z_2}{Z_1} = \frac{U_2}{U_1}. \tag{2}$$

The bridge networks of Z_1 and Z_2 consist of slightly different components, such as cables, connectors, and equalizers. To minimize these systematic errors, measurements are performed in both the 'forward' (F) and 'reverse' (R) configurations [11] by means of coaxial switches. It is important to note that the error suppression is only applied for the networks before the switches. Thus, errors from the network after the switches, particularly at sensitive branches (HP and LC), must be encountered in cable correction or incorporated into the uncertainties [4].

Coaxial switches F1 and R1 are activated in the forward configuration, while F2 and R2 are deactivated. Under these conditions, Z_1 is linked to U_1 and Z_2 to U_2, enabling the computation of the forward ratio $(Z_2/Z_1)_{\mathrm{F}}$. In the reverse configuration, switches F2 and R2 are on, with F1 and R1 off, resulting in an exchange in the applied voltages. Hence Z_1 is connected to U_2 and Z_2 to U_1, facilitating the computation of the reverse ratio $(Z_2/Z_1)_{\mathrm{R}}$.

After each voltage interchange, the bridge is fully rebalanced. The final ratio is determined by taking the geometric average of the measurements obtained in both the forward and reverse directions, as expressed:

$$\frac{Z_2}{Z_1} = \sqrt{\left(\frac{Z_2}{Z_1}\right)_{\mathrm{F}} \left(\frac{Z_2}{Z_1}\right)_{\mathrm{R}}}. \tag{3}$$

Equations (1)–(3) can be applied to both ratio and quadrature measurements.

For the QHR-related measurements, the triple-series connections of the QHR eliminate the need for a Kelvin network [19]. Hence, the balancing procedure is simpler, involving adjustments to the currents in the HP arms and the primary balance. By employing equation (4), the impedance value linked to the QHR can be determined.

$$Z = \left(\frac{U_2}{U_1} + \frac{U_{\mathrm{D}}}{U_1} S\right) R_{\mathrm{H}} \tag{4}$$

Here, Z represents the impedance value, S stands for the sensitivity coefficient. U_{D} is the detected output, while U_1 and U_2 represent the applied voltages from each JAWS. R_{H} denotes the QHR and is defined as $R_{\mathrm{K}}/2$. The von Klitzing constant R_{K} equals h/e^2, h is the Plank's constant, and e is the elementary charge.

3. Uncertainties

The uncertainties for R:R and C:C were evaluated across a frequency range from 53 Hz to 50 kHz. The measurement models outlined in equations (5) and (6) were employed to determine the combined uncertainties. The calculations followed the guide to the expression of uncertainty in measurement (GUM) guidelines [20].

The mathematical model for the ratio and quadrature measurements is given by:

$$\begin{aligned} R + \Delta R = &\left(U_{\mathrm{ratio}} + \Delta U_{\mathrm{JAWS}} + \Delta U_{\mathrm{cable}}\right) \\ &\times \left(1 + M + K + \Delta B\right), \end{aligned} \tag{5}$$

with $R = Z_2/Z_1$, $U_{\mathrm{ratio}} = U_2/U_1$, $M = (U_{\mathrm{D1}}/S_{\mathrm{N1}} + U_{\mathrm{D2}}/S_{\mathrm{N2}})/2$, and $K = (U_{\mathrm{D1}}/S_{\mathrm{K1}} – U_{\mathrm{D2}}/S_{\mathrm{K2}})/2$. The combined uncertainty of the ratio ΔR is determined by incorporating ΔU_{JAWS} from JAWS, $\Delta U_{\mathrm{cable}}$ from cable correction, and ΔB from bridge deviation.

The mathematical model for the QHR setup:

$$\begin{aligned} Q + \Delta Q = &\left(U_{\mathrm{ratio}} + \Delta U_{\mathrm{JAWS}} + \Delta U_{\mathrm{cable}} + D + \Delta D\right) \\ &\times \left(1 + \Delta f_{\mathrm{QHR}}\right). \end{aligned} \tag{6}$$

Where $Q = Z/R_{\mathrm{H}}$, $U_{\mathrm{ratio}} = U_2/U_1$, and $D = (U_{\mathrm{D}} \cdot S/U_1)$. The combined uncertainty of the ratio ΔQ is determined by incorporating ΔU_{JAWS} from JAWS, $\Delta U_{\mathrm{cable}}$ due to cable correction, ΔD from bridge deviation and Δf_{QHR} corresponds to the frequency-dependent characteristics of the QHR.

Details of each uncertainty component are described below.

- Bridge resolution

The resolution of a bridge is categorized as a type A uncertainty. The accumulated noise at the detection point influences its value. The noise primarily originates from the Johnson noise of resistive components and the input noise of the amplifier before the detector. An Allan variance analysis was conducted over 30 min to assess the bridge's resolution [10, 21]. At 1233.15 Hz, when measuring the ratio of two capacitors, the bridge achieved a type A uncertainty of less than 1 nV V^{-1} after 60 s of measurement time.

- JAWS voltage (ΔU_{JAWS})

This component is attributed to amplitude errors from the JAWS due to the effects of array inductance and crosstalk between the arrays. The inductances of the arrays are typically within the range of (15.5–18.5) nH [22–24]. However, these inductive errors can be suppressed by implementing forward and reverse measurements [11]. To reduce the crosstalk issue, specialized copper enclosures were employed to shield the arrays [10]. The remaining effects were evaluated to have an error below 1 nV V^{-1} at 1233.15 Hz.

- Cable corrections ($\Delta U_{\mathrm{cable}}$)

The measurement results from a bridge can be influenced by the cable's admittance (Y) and impedance (Z), especially in the HP and LC arms [4]. Cable corrections are applied to the reported ratios for the HP arms involved in the networks after the switches and the LC arms from the Kelvin sources to the LC ports of the impedance standards.

It is essential to consider residual errors since the actual impacts of the Y and Z components on the bridge may deviate from the measured values. The Y and Z were obtained using a digital impedance meter. Therefore, the uncertainty components were calculated by multiplying the meter's relative accuracies with the correction values. For frequencies up to 10 kHz, the uncertainties remained below 3 n$\Omega\,\Omega^{-1}$.

- Bridge deviation (ΔB or ΔD)

This error is attributed to current imbalances within the HP terminals and the Kelvin network. Intentional imbalance measurements were employed to determine these values.

- Frequency dependence of the QHR (Δf_{QHR})

In AC applications involving the QHR, a frequency dependence of the Hall resistance is evident in graphene devices (without applying an active potential to a double shield [3]). For the utilized sample, this characteristic was quantified below 80 nΩ (Ω·kHz)$^{-1}$ and used for corrections. However, it is essential to account for the error when assessing uncertainty, as the long-term characteristics of samples are not known yet. The estimated value of this error is 23 nΩ (Ω·kHz)$^{-1}$.

Table 1. Uncertainty budget for 10 nF:10 nF ratio measurements at frequencies from 53 Hz to 50 kHz with nominal applied voltages of 100 mV. The relative uncertainties are in $\mathrm{nF\,F^{-1}}$ with $k = 1$.

Component	53 Hz[1]	1.2 kHz[2]	30 kHz[2]	50 kHz[3]
Bridge resolution	1	<1	4	7
JAWS voltage	<1	<1	12	19
Cable correction	<1	<1	3	7
Bridge deviation	4	2	33	184
Combined	5	2	36	185

Table 2. Uncertainty budget for 12.9 kΩ:10 kΩ ratio measurements at frequencies from 53 Hz to 50 kHz with nominal applied voltages of 100 mV and ≈77 mV. The relative uncertainties are expressed in $\mathrm{n\Omega\,\Omega^{-1}}$ with $k = 1$.

Component	53 Hz[1]	1.2 kHz[2]	30 kHz[2]	50 kHz[2]
Bridge resolution	4	3	5	5
JAWS voltage	<1	<1	12	20
Cable correction	<1	<1	3	8
Bridge deviation	3	1	4	8
Combined	5	4	14	24

Tables 1 and 2 show the combined uncertainties with a coverage factor (k) of 1 for the 10 nF:10 nF ratio and 12.9 kΩ:10 kΩ ratio measurements. For all stated values and uncertainties, we averaged five sets of forward and reverse measurements.

Remarks [1], [2], and [3] indicate that the uncertainties were derived from different setups. Detailed information on each setup can be found in section 5.1.

The combined uncertainty for R:$(1/\omega C)$ is $9\,\mathrm{n\Omega\,\Omega^{-1}}$ and for an impedance linked to the graphene AC QHR is $23\,\mathrm{n\Omega\,\Omega^{-1}}$. These uncertainties were determined at 1233.15 Hz with nominal applied voltages of 100 mV, by the bridge configuration described in [13].

4. Standards

4.1. Impedance standards

Four impedance standards were used, consisting of two 10 nF capacitance standards, a 10 kΩ resistance standard, and a 12.9 kΩ resistance standard. Each 10 nF standard was assembled by combining four commercial 10 nF capacitors in series and parallel. Similarly, each resistance standard was built by connecting four commercial resistors in series. All four standards are enclosed, each in an airtight aluminum housing. The temperature inside the housing is regulated using a two-stage thermostat, maintaining a constant temperature of around 30 °C with high stability within the millikelvin range.

Over three years, the long-term stabilities of these standards have been monitored through periodic calibrations. The 10 nF capacitance standards were calibrated against PTB's QHR using traditional IVD-based bridges. Both capacitance values exhibited a daily drift rate of less than $-1\,\mathrm{nF\,F^{-1}}$. The resistance standards were calibrated using PTB's cryogenic current comparator (CCC), resulting in a daily drift rate of approximately $-2.3\,\mathrm{n\Omega\,\Omega^{-1}}$.

4.2. AC QHR standard

Graphene-based QHR devices can operate over various temperatures and magnetic fields, providing high adaptability and operational convenience. A graphene device doped with F4-TCNQ molecules, utilized in this setup, was fabricated at PTB [25]. The device featured six terminals and was mounted on a TO-8. Incorporating fewer Hall contacts in the design aimed to minimize the device's capacitive loss characteristics, which influences the measurement results in the AC applications.

The device was immersed in a cryomagnetic system cooled by liquid helium. The system can be operated with a maximum magnetic field of ±7 T. We conducted DC magnetotransport measurements of the Hall resistance (R_{xy}) and the longitudinal resistivity (ρ_{xx}) to analyze the characteristics of the device. This analysis assessed the charge carrier density and mobility. The charge carrier density was $p = 5.5 \times 10^{10}\,\mathrm{cm^{-2}}$ and carrier mobility was on the level of $\mu = 5900\,\mathrm{cm^2\,V^{-1}s}$. The DC characterization displayed the resistance plateau between −2 T to −7 T, with the lowest longitudinal resistivity observed at −5 T. Detailed information on the characterization measurements for this device can be found in [14].

The AC characteristics of the sample were assessed by examining its magnetic field dependencies at a frequency of 1233.15 Hz. To determine the AC Hall resistance, quadrature measurements were carried out, comparing a 10 nF capacitance standard with the QHR using the 4TP Josephson bridge.

The procedure began by balancing the bridge at the maximum magnetic field of −7 T. Subsequently, the magnetic field was gradually varied from −7 T to −3.5 T at a rate of 0.075 T per min, with no further adjustments to the bridge's balance. Figure 2 illustrates the deviations of the AC Hall resistance ($\triangle R_{\mathrm{xy}}$) compared to the quantized DC value ($R_{\mathrm{K}}/2$) during the field sweep. The average deviation between magnetic field strengths of −7 T and −5 T is $85\,\mathrm{n\Omega\,\Omega^{-1}} \pm 23\,\mathrm{n\Omega\,\Omega^{-1}}$. The uncertainty was considered from the bridge, and the uncertainty in extrapolating the reference value for the 10 nF capacitance standard.

Considering the outcomes from the AC approach in conjunction with the DC characteristics, the magnetic field at −5 T was selected as the operation point for this sample.

5. Measurement results

Various measurements were conducted to assess the performance as well as the reproducibility and consistency of the bridge.

For consistency checks, 'triangle' measurements were conducted [26]. This method was selected due to its unique advantages, such as eliminating the requirement for a reference value.

The triangle measurements incorporate ratio and quadrature configurations. The ratio measurement involved

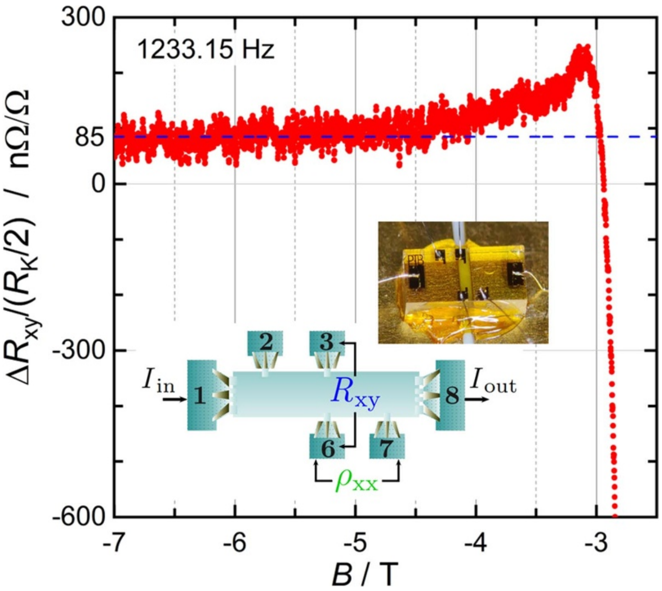

Figure 2. Difference of the measured AC Hall resistance ($\triangle R_{xy}$) compared to the DC Hall resistance ($R_K/2$) as the magnetic field is varied. Quadrature measurements were conducted between a 10 nF capacitance standard compared with the QHR to access the measured Hall resistance. The image inside the plot displays a PTB's graphene Hall device without the TO-8 holder. The device's schematic outlines the current contacts (1 and 8), high-potential contacts (2 and 3), and low-potential contacts (6 and 7).

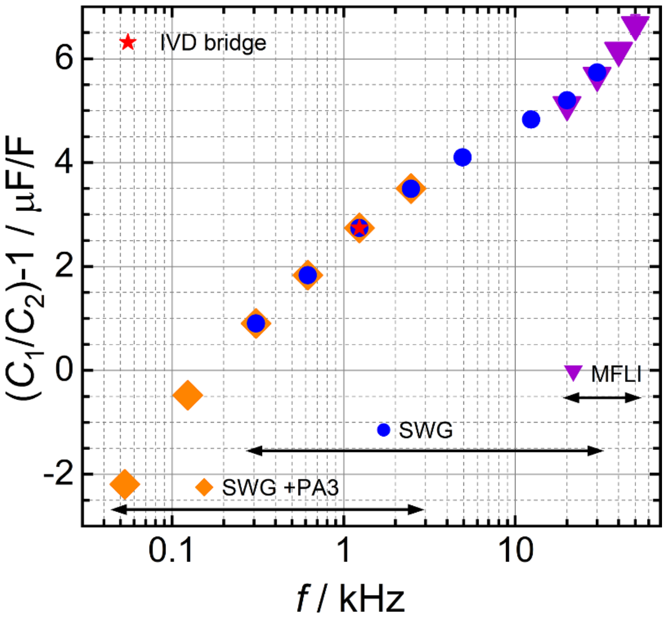

Figure 3. Deviation of 10 nF:10 nF ratios from the nominal. The ratios were measured by the 4TP Josephson impedance bridge with three sub-setups. The measurements were conducted at nominal applied voltages of 100 mV at a frequency range from 53 Hz to 50 kHz. The data obtained from the 'SWG + PA3' setup are represented by orange diamonds, 'SWG' by blue circles, and 'MFLI' by purple downward triangles. The PTB's IVD bridge provided a reference point as a red star at 1233.15 Hz.

comparing the 12.9 kΩ resistance standard to the graphene AC QHR at 1233.15 Hz. The result is expressed as $R_H/R_{12.9\,k\Omega}$. Quadrature measurements were also performed at the same frequency. The first set of measurements compared the 10 nF capacitor to the 12.9 kΩ resistor, expressed as $R_{12.9\,k\Omega}/Z_{C2}$, and the second set of measurements linked the 10 nF capacitance standard to the QHR, represented as Z_{C2}/R_H.

To check if the bridge is operating as expected, we verified if the product of these three measurements $(R_H/R_{12.9\,k\Omega}) \times (R_{12.9\,k\Omega}/Z_{C2}) \times (Z_{C2}/R_H)$ is 1. In our measurements, the product deviated from the expected value by 36 nΩ Ω^{-1}, with an associated standard uncertainty of 16 nΩ Ω^{-1} [14]. The triangle check was repeated within the same week, resulting in a slight difference of 1 nΩ Ω^{-1} compared to the initial check.

5.1. Capacitance ratio measurements

Two 10 nF capacitance standards were compared in a 1:1 ratio, with applied nominal voltages of 100 mV. The deviations of ratios from the nominal value $[(C_1/C_2) - 1]$ were observed using the Josephson bridge in three different sub-setups[1, 2 & 3].

The first setup, 'SWG + PA3[1],' involved a modular sine wave generator (SWG) as an integral component of the current sources. The SWG was developed by the Czech Metrology Institute (CMI) [27]. Additionally, signals detected at detectors D_{HP1} and D_{HP2} were amplified 60 times using PTB's ultra-low noise AC-preamplifiers model 3 (PA3). Measurement ratios in the frequency range from 53 Hz to 2.5 kHz are illustrated as orange diamonds in figure 3. At these lower frequency ranges, the sensitivities at the D_{HP} detectors are small. Thus, amplifying the signals is essential to achieve a more accurate balance.

In the second setup labeled 'SWG[2],' the SWG acted as the current source without any signal amplification at D_{HP}. Blue circles represent ratios ranging from 308 Hz to 30 kHz. In the last setup, 'MFLI[3],' current sources were implemented using LIAs of the Zurich Instruments[†] MFLI model. With this setup, measurements extended from 20 kHz to 50 kHz and are indicated by purple downward triangles. The LIA was employed instead of the SWG due to the limited performance of the SWG source when conducting capacitance ratio measurements within these frequency ranges. The exact causes of this limitation have not been fully determined yet, but it may arise due to the high current requirements for low impedance and high-frequency measurements.

All observed values were adjusted for cable corrections and are presented with combined standard uncertainties. The uncertainty bars included in the plot are smaller than the data point sizes. The relative combined uncertainty and its components from the 'SWG + PA3' and 'SWG' configurations can be viewed in figure 4. The associated uncertainties for these plots are provided in table 1.

A red star symbolizes the result obtained through the PTB's traditional IVD bridge at 1233.15 Hz. At this frequency, the

[†] Identification of commercial equipment does not imply recommendation or endorsement by PTB, nor does it imply that the equipment is necessarily the best available for the purpose.

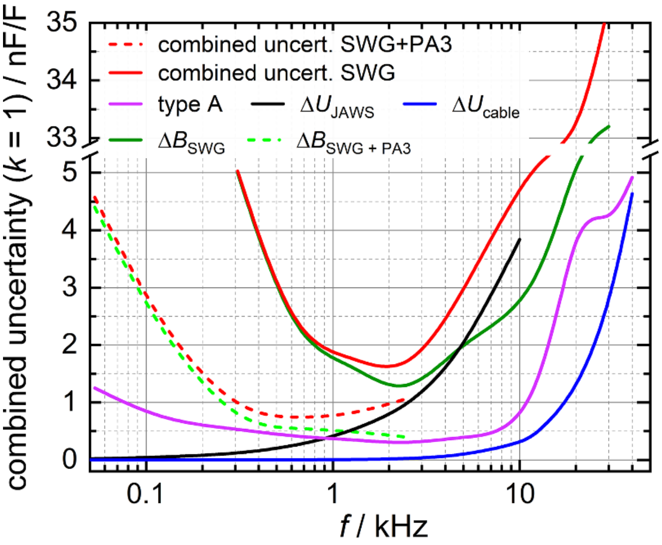

Figure 4. The plot represents the spline interpolation for the relative combined uncertainty for the 10 nF:10 nF ratios and its components over the measured frequency range for bridge configurations 'SWG + PA3' and 'SWG' setups. The combined uncertainties of the bridge configuration 'MFLI' is dominant. Thus, they are not included in the plot for a clearer presentation.

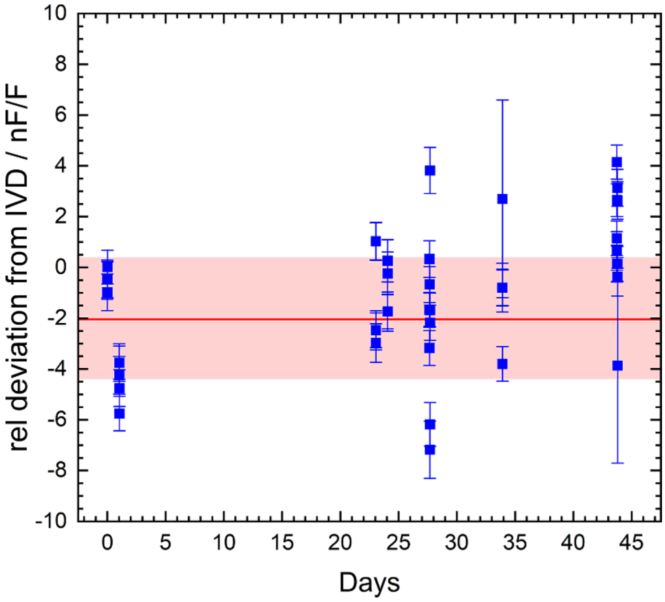

Figure 5. The deviation of the 10 nF:10 nF ratios obtained by the Josephson impedance bridge from the IVD value at 1233.15 Hz. The red line presents the average deviation of approximately -2 nF F^{-1}. The error bars are type A, and the red area indicates the standard deviation of all data. The measurements were observed over 45 days.

values from the Josephson and the IVD bridges exhibit exceptional agreement of 1 nF F^{-1} with a combined standard uncertainty of 3 nF F^{-1}. When discussing the combined uncertainties for calculated results, such as deviation values, it is essential to recognize that these uncertainties are derived from both the Josephson bridge and the bridge being compared, in this instance, the IVD bridge.

To ensure the reproducibility of the Josephson bridge, we conducted multiple capacitance ratio measurements over 45 days. Figure 5 illustrates the relative deviation of the measured $[(C_1/C_2) - 1]$ from the IVD values at 1233.15 Hz. The error bars represent type A, and the red line represents the average deviation, approximately -2 nF F^{-1}. The standard deviation of all the collected data is highlighted in red light-shaded area. The points with unusually large type A are observed simultaneously in both outputs, which could be caused by external interference.

5.2. Resistance ratio measurements

Measurements of 12.9 kΩ:10 kΩ resistance ratios were conducted across a frequency range from 53 Hz to 50 kHz. The JAWS system applied two different outputs: a 100 mV signal to the 12.9 kΩ resistance standard and an ≈77 mV signal to the 10 kΩ resistance standard. Two setups, 'SWG + PA3' and 'SWG,' as depicted above, were utilized in the experiment.

Figure 6 displays the relative differences of 12.9 kΩ:10 kΩ ratios obtained from the Josephson bridge compared to the CCC ratio measured using DC voltage. The 'SWG + PA3' configuration results are represented by orange diamonds, covering a frequency range from 53 Hz to 2.5 kHz. The 'SWG' configuration results are depicted as blue circles, spanning

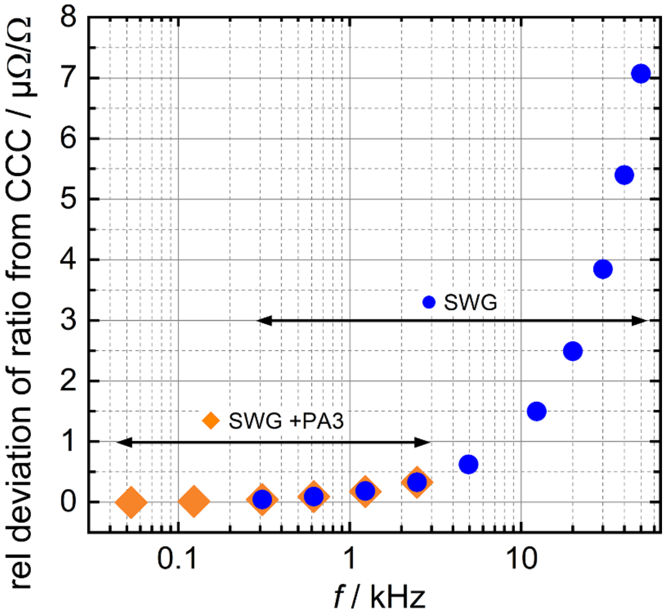

Figure 6. Deviation of 12.9 kΩ:10 kΩ ratios from the CCC value. The ratios were measured by the 4TP Josephson impedance bridge for frequencies ranging from 53 Hz to 50 kHz. The values from the 'SWG + PA3' setup are presented in orange diamonds. The ratios achieved from the 'SWG' setup are shown in blue circles.

a frequency range from 308 Hz to 50 kHz. These observed values were adjusted by cable corrections and are presented with combined standard uncertainties. The uncertainty bars shown in the graph are smaller than the sizes of the data points. Figure 7 shows the relative combined uncertainty and

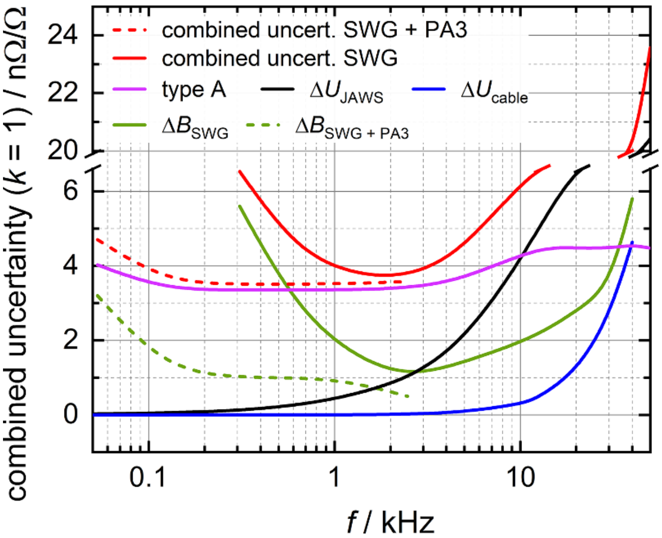

Figure 7. The plot represents the spline interpolation for the relative combined uncertainty for the 12.9 kΩ:10 kΩ ratios and its components as a function of frequency for bridge configurations 'SWG + PA3' and 'SWG' setups.

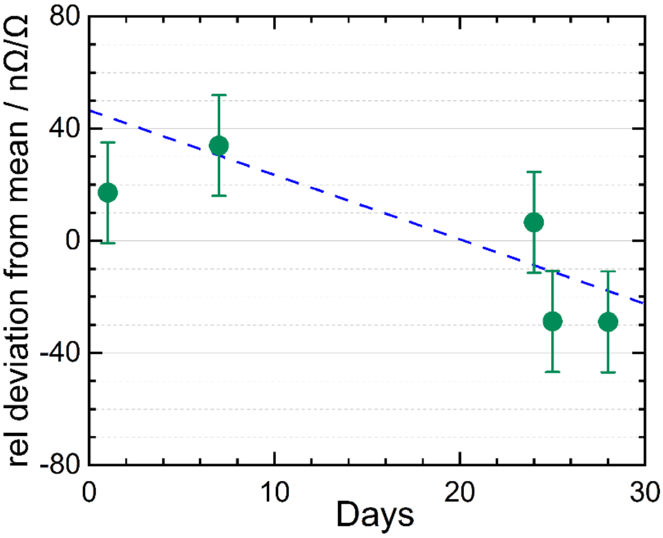

Figure 8. The 12.9 kΩ resistance standard was compared to the graphene AC QHR at 1233.15 Hz. The deviations of the measured resistance from the mean value were observed within 28 days, as depicted by the green circles. The error bars indicate the combined standard uncertainties. The dashed line presents the drift of the 12.9 kΩ resistor determined by the CCC.

its components. The associated uncertainties for these measurements are provided in table 2.

At 53 Hz, the measured ratio by the Josephson bridge deviated from the DC ratio, observed by the CCC, by $-2\,\mathrm{n}\Omega\,\Omega^{-1} \pm 5\,\mathrm{n}\Omega\,\Omega^{-1}$ ($k = 1$).

5.3. Quadrature measurements

The bridge can easily modify the phase between the JAWS voltage signals. Therefore, the quadrature impedance bridge can be functioned using the same setup as the ratio bridge.

Two quadrature measurement sets were conducted to compare resistance and capacitance standards. These measurements were carried out at 1233.15 Hz with nominal supplied voltages of 100 mV. The first set of measurements compared a 10 nF capacitance standard labeled as C_1 and the 12.9 kΩ resistance standard. The second measurement set followed the same procedure but with a different 10 nF capacitance standard labeled as C_2. These measurements [12.9 kΩ:($1/\omega C_x$)] allowed for calculating a deviation of the indirect ratio from the nominal value $[(C_1/C_2) - 1]$. The Josephson bridge yielded a result of 2.502 $\mu\mathrm{F}^{-1}$, with a standard uncertainty of 13 nF F^{-1}. Value obtained from the IVD-based bridge was 2.507 $\mu\mathrm{F}^{-1}$ with a standard uncertainty of 2 nF F^{-1}.

5.4. Impedance standard link to the graphene AC QHR

Capacitance and resistance standards were directly compared to the graphene AC QHR at 1233.15 Hz. Furthermore, quadrature measurements were performed using similar approaches to the measurements in the section 5.3. The first set of comparisons involved C_1 and the QHR, while in the second series, C_2 was compared against the QHR. The QHR device employed a magnetic field strength of −5 T. The $[(C_1/C_2) - 1]$ agreed well with the results presented above and is 2.516 $\mu\mathrm{F}^{-1}$, with a combined standard uncertainty of 13 nF F^{-1}.

Reproducibility checks were conducted by comparing the 12.9 kΩ resistance standard to the QHR at a frequency of 1233.15 Hz over a period of 28 days. Figure 8 presents the relative deviations of the measured resistance from the mean value. The error bars represent a combined standard uncertainty of 23 nΩ Ω^{-1}. The dashed line illustrates the drift of the 12.9 kΩ resistance standard determined by the CCC bridge.

6. Conclusion

We have presented a fully automated 4TP Josephson impedance bridge using pulse-driven Josephson voltage standards. A single bridge configuration can be used to determine ratios of like impedances, R:R and C:C, and for quadrature measurements. Direct comparisons of resistance and capacitance impedance standards to a graphene AC QHR have also been performed. Furthermore, small changes allow this bridge to measure in the frequency range from 53 Hz to 50 kHz.

The agreement of the results for the 10 nF:10 nF ratio with those from an IVD-based ratio bridge is better than 1 nF $\mathrm{F}^{-1} \pm 3$ nF F^{-1} ($k = 1$) at 1233.15 Hz. The 12.9 kΩ:10 kΩ ratios have been measured over the same frequency range. At 53 Hz, the ratio deviates from the DC value, obtained by the CCC, by $-2\,\mathrm{n}\Omega\,\Omega^{-1} \pm 5\,\mathrm{n}\Omega\,\Omega^{-1}$ ($k = 1$).

Indirect $[(C_1/C_2) - 1]$ results via 12.9 kΩ:($1/\omega C_x$) ratios using the resistance standard and via QHR-linked measurements, although not compensated for its frequency dependence, agreed with the values determined with the IVD-based bridge within 9 nF $\mathrm{F}^{-1} \pm 13$ nF F^{-1} ($k = 1$). Furthermore, we examined the consistency and reproducibility of the Josephson impedance bridge over 45 days, and the 10 nF:10 nF ratio agreed within the uncertainty of 3 nF F^{-1}.

Moreover, the evaluation of the combined uncertainty for 10 nF:10 nF and 12.9 kΩ:10 kΩ ratios, as well as for quadrature shows that the Josephson 4TP bridge is competitive with state of the art IVD bridges. At 1233.15 Hz, the standard uncertainties are 2 nF F^{-1} and 4 nΩ Ω^{-1}, respectively. The uncertainty of the R:$(1/\omega C)$ and R:R measurements that involved the graphene AC QHR are dominated by its frequency dependence contribution as we did not employ the double shield technique.

In the future, this dominant contribution will be tackled by implementing double shields in our graphene sample holder. We will investigate the frequency dependence of AC QHR up to the maximum operating frequency of the Josephson bridge, 50 kHz. We will also validate the capacitance and resistance calibrations with our new automated Josephson impedance bridge above 5 kHz by means of comparisons with other broadband impedance bridges.

Acknowledgments

The authors would like to extend their thanks to Jürgen Schurr, Martin Götz, Jinni Lee, and Eckart Pesel for their calibration support, as well as Hansjörg Scherer, Yefei Yin, Atasi Chatterjee, Klaus Pierz, Jan Kučera, Susanne Gruber, Michael Busse, Torsten Stöcker, Niklas Abraham, Judith Felgner, Rolf Gerdau, Gerhard Muchow, Kathrin Störr, Thomas Weiman for their support and technical assistance. This work received partial funding from the GIQS-Graphene Impedance Quantum Standard project, supported by the EMPIR programme, co-financed by the Participating States and the European Union's Horizon 2020 research and innovation programme. Furthermore, we appreciate the support provided to Yaowaret Pimsut by the International Graduate School of Metrology (IGSM) at the Technische Universität Braunschweig.

ORCID iDs

Yaowaret Pimsut https://orcid.org/0000-0001-9210-6512
Stephan Bauer https://orcid.org/0000-0001-6242-2223
Marco Kraus https://orcid.org/0000-0002-7592-9493
Ralf Behr https://orcid.org/0000-0002-5480-443X
Mattias Kruskopf https://orcid.org/0000-0003-2846-3157
Oliver Kieler https://orcid.org/0000-0001-5193-8910
Luis Palafox https://orcid.org/0000-0001-7663-856X

References

[1] Overney F and Jeanneret B 2018 Impedance bridges: from Wheatstone to Josephson *Metrologia* **55** S119
[2] Kibble B P and Rayner G H 1984 *Coaxial AC Bridges* (Adam Hilger Ltd.)
[3] Schurr J, Bürkel V and Kibble B P 2009 Realizing the farad from two ac quantum Hall resistances *Metrologia* **46** 619–28
[4] Awan S, Kibble B P and Schurr J 2010 *Coaxial Electrical Circuits for Interference-Free Measurements* (The Institution of Engineering and Technology)
[5] Lee J, Schurr J, Nissilä J, Palafox L and Behr R 2010 The Josephson two-terminal-pair impedance bridge *Metrologia* **47** 453–9
[6] Hagen T, Palafox L and Behr R 2017 A Josephson impedance bridge based on programmable Josephson voltage standards *IEEE Trans. Instrum. Meas.* **66** 1539–45
[7] Palafox L, Behr R, Nissilä J, Schurr J and Kibble B P 2012 Josephson impedance bridges as universal impedance comparators *Conf. on Precision Electromagnetic Measurements CPEM Digest* pp 464–5
[8] Benz S P and Hamilton C A 1996 A pulse-driven programmable Josephson voltage standard *Appl. Phys. Lett.* **68** 3171–3
[9] Benz S P, Burroughs C J and Dresselhaus P D 2000 Low harmonic distortion in a Josephson arbitrary waveform synthesizer *Appl. Phys. Lett.* **77** 1014–6
[10] Bauer S, Behr R, Hagen T, Kieler O, Lee J, Palafox L and Schurr J 2017 A novel two-terminal-pair pulse-driven Josephson impedance bridge linking a 10 nF capacitance standard to the quantized Hall resistance *Metrologia* **54** 152–60
[11] Overney F, Flowers-Jacobs N E, Jeanneret B, Rüfenacht A, Fox A E, Dresselhaus P D and Benz S 2020 Dual Josephson impedance bridge: towards a universal bridge for impedance metrology *Metrologia* **57** 065014
[12] Overney F, Flowers-Jacobs N E, Jeanneret B, Rüfenacht A, Fox A E, Underwood J M, Koffman A D and Benz S P 2016 Josephson-based full digital bridge for high-accuracy impedance comparisons *Metrologia* **53** 1045
[13] Bauer S *et al* 2021 A four-terminal-pair Josephson impedance bridge combined with a graphene quantized Hall resistance *Meas. Sci. Technol.* **32** 065007
[14] Marzano M, Pimsut Y, Kruskopf M, Yin Y, Kraus M, D'Elia V, Callegaro L, Ortolano M, Bauer S and Behr R 2022 PTB-INRIM comparison of novel digital impedance bridges with graphene impedance quantum standards *Metrologia* **59** 065001
[15] Kováč J and Kučera J 2015 A modular coaxial multiplexer with high isolation between channels *XXI IMEKO World Congress 'Measurement in Research and Industry' (Prague, Czech Republic, 30 August–04 September 2015)* (available at: https://www.imeko.org/publications/wc-2015/IMEKO-WC-2015-TC4-127.pdf)
[16] Schurr J and Melcher J 2004 Unequalized currents in coaxial ac bridges *IEEE Trans. Instrum. Meas.* **53** 807–11
[17] Kieler O F, Behr R, Wendisch R, Bauer S, Palafox L and Kohlmann J 2014 Towards a 1 V Josephson arbitrary waveform synthesizer *IEEE Trans. Appl. Supercond.* **25** 1400305
[18] Benz S P, Burroughs C J and Dresselhaus P D 2001 AC coupling technique for Josephson waveform synthesis *IEEE Trans. Appl. Supercond.* **11** 612–6
[19] Delahaye F 1993 Series and parallel connection of multiterminal quantum Hall-effect devices *J. Appl. Phys.* **73** 7914–20
[20] BIPM, IEC, IFCC, ILAC, ISO, IUPAC, IUPAP and OIML 2008 Evaluation of measurement data–guide to the expression of uncertainty in measurement *Joint Committee for Guides in Metrology, JCGM* 100:2008 1st edn
[21] Witt T J 2007 Using the autocorrelation function to characterize time series of voltage measurements *Metrologia* **44** 201
[22] Burroughs C J, Benz S P and Dresselhaus P D 2003 AC Josephson voltage standard error measurements and analysis *IEEE Trans. Instrum. Meas.* **52** 542–4

[23] Landim R P, Benz S P, Dresselhaus P D and Burroughs C J 2008 Systematic-error signals in the AC Josephson voltage standard: measurement and reduction *IEEE Trans. Instrum. Meas.* **57** 1215–20

[24] Underwood J M 2019 Uncertainty analysis for ac–dc difference measurements with the AC Josephson voltage standard *Metrologia* **56** 015012

[25] Yin Y, Chatterjee A, Momeni D, Kruskopf M, Götz M, Wundrack S, Hohls F, Pierz K and Schumacher H W 2022 Tailoring permanent charge carrier densities in epitaxial graphene on SiC by functionalization with F4-TCNQ *Adv. Phys. Res.* **1** 2200015

[26] Musioł K and Kampik M 2019 Metrological triangles in impedance comparisons *Measurement* **148** 106908

[27] Kučera J, Kováč J, Palafox L, Behr R and Vojáčková L 2020 Characterization of a precision modular sinewave generator *Meas. Sci. Technol.* **31** 064002